Deformability and solvent penetration in soft nanoparticles at liquid-liquid interfaces

Daniel J. Arismendi-Arrieta*,† and Angel J. Moreno*,‡,†

†*Donostia International Physics Center (DIPC), Paseo Manuel de Lardizabal 4, E-20018 San Sebastián, Spain*

‡*Centro de Física de Materiales (CSIC, UPV/EHU) and Materials Physics Center MPC, Paseo Manuel de Lardizabal 5, E-20018 San Sebastián, Spain*

E-mail: darismendi@dipc.org; angeljose.moreno@ehu.eus

Abstract

Soft nanoparticles hold promise as smart emulsifiers due to their high degree of deformability, permeability and stimuli responsive properties. By means of large-scale simulations we investigate the structural properties of nanogels at liquid-liquid (A-B) interfaces and the miscibility of the liquids inside the nanogels, covering the whole range of interfacial strength from the limit of single-liquid to the case of stiff interfaces. To study the role of the internal architecture and deformability of the nanogel we simulate a realistic disordered and an ideal regular network, for a broad range of cross-linking degrees. Unlike in previous investigations on liquid miscibility, excluded volume interactions are considered for both the monomers and the explicit solvent particles. The nanogel permeability is analysed by using an unbiased grid representation that accounts for the surface fluctuations and adds to the density profiles the exact number of liquid particles inside the nanogel. The better packing efficiency of the regular network leads

to higher values of the total liquid uptake and the invasive capacity (A-particles in B-side and *viceversa*) than in the disordered network, though differences vanish in the limit of rigid interfaces. Uptake and invasion are optimized at a cross-linking degree that depends on the interfacial strength, tending to $\sim 15-20$ for moderate and stiff interfaces. As the interfacial strength increases, the miscibility inside the nanogel is enhanced by a factor of up to 5 with respect to the bare interface, with the disordered networks providing a better mixing than their ideal counterparts. The emerging scenario reported here provides general guidelines for tuning the shape, uptake, invasive, and mixing capacities of nanogels adsorbed at liquid-liquid interfaces.

1 Introduction

Crosslinked polymeric particles represent a special class of soft colloids with the ability of adapting their dimensions according to the surrounding environment or via an external stimulus.[1–3] So far, very attractive applications derived from nanogels and microgels in suspensions or at fluid-fluid interfaces have been proposed such as: controlled drug delivery, catalysis, antifouling coatings, cell encapsulation and tissue engineering, among others. [4–7] Deformability, especially at interfaces, is the most differentiating feature with respect to core-shell colloids and truly hard solid particles.[8] Due to their intrinsic stimuli-responsive properties they may prove beneficial in a wide range of technologies such as thermocromic components in smart windows,[9] high-performance bio-lubricants,[10] controlling the metastability of emulsions and foams,[11] directing self-assembly processes,[12] or even as models for translating our current understanding of submicron synthetic gels into food based systems.[13,14]

In the context of the oil-water interface, emulsion stabilization still remains as a very active research field with novel concepts constantly being introduced.[15–17] For instance, solid particles continue to being explored for understanding their active or passive role in the self-fragmentation process of armored droplets,[18] while the interfacial behavior of more complex particles has been considered only recently.[19] Current efforts are focused on designing

responsive emulsions that stabilize or break on demand[20] with the help of smart emulsifiers. Therefore, the inherent interfacial activity and stimuli-sensitive properties of soft particles could facilitate the control and formation of responsive elastic barriers that interfere with coalescence and ripening type processes.[11] However, given the multifactorial character of this problem, studies very often rationalize their results by varying one parameter at the time and consequently few attempts have been made to characterize such systems in a general way.[11]

It is clear that understanding the way such particles deform on adsorption at interfaces is very important from the fundamental and applied point of view. Nevertheless, our ability to make, measure and modelling these objects is nowadays the principal limiting factor. With the advances in synthesis methods, it is possible to design microscale particles with complex architectures.[21] Nevertheless, for the case of nanoscale analogous, it is still very challenging to generate tailored internal topologies and more importantly to maintain a uniform size distribution. Additionally, if internal structure details are required, then they are very difficult to be detected by experimental techniques as deformability introduces additional degrees of freedom that current measurements hardly distinguish. Even with the arrival of super-resolution microscopic techniques,[22,23] a detailed topological characterization of microgels is still scarce, and in the case of nanogels non-existent. Only few experimental studies have quantified the location of microgels at liquid-liquid interfaces by introducing the concept of two contact angles on lens-like shape particles.[24,25] This however rises the question if due to the solvent penetrability the definition of any contact angle has any sense in such systems.[11,14] Anyhow, it is evident that alternative approaches are required to understand particle conformations at interfaces.

On the other hand, computer simulations allow to correlate such aspects in a more controlled way and ultimately generate predictions with respect to properties that are hardly reachable by the lack of experimental resolution. In doing so two elements have to be considered: i) how to model the solvent and ii) how realistic the internal nanoparticle's architecture

has to be. For the first element, two approaches are often used to deal with explicit solvent simulations: molecular dynamics (MD) of particles with excluded volume interactions, and dissipative particle dynamics (DPD) with bounded potentials.[1,26,27] The latter, as a mesoscopic simulation approach, allows for a direct mapping to Flory-Huggins lattice models and has been recently employed to understand swelling or deswelling of microgels at suspensions,[28] and their behavior at liquid interfaces.[29–33] The former is rarely used due to its huge computational cost, originating from the longer diffusion times required with respect to the case of fully penetrable DPD particles. Regarding the second element, a critical point in current models is that a regular network (e.g. diamond lattice) is usually assumed within such soft nanoparticles, whereas with traditional synthetic approaches a very disordered network abundant in defects (e.g. loops) is formed.[34] The use of excluded volume interactions between the nanogel's monomers is also essential in modelling realistic nanogels. Whereas in the case of regular diamond networks the use of DPD interactions for both the liquid and the monomers[30,31,33] might still be sufficient to model their spatial distribution, such interactions are clearly inadequate for the monomers in the disordered networks. An increasing number of permanent contacts (entanglements) between neighboring strands is expected by increasing the degree of cross-linking, or just by flatening of the nanogel in the interface. In such conditions the bounded character of the DPD interactions will easily lead to violation of the topological constraints through chain crossing. Modelling of realistic microgel networks poses a computational challenge for developing suitable *in-silico* protocols that best mimic the internal microgel's structure, density profiles, form factors, as well as the kinetics of swelling and deswelling found at different experimental conditions. Several efforts to provide realistic models have been reported very recently.[34–38] See, e.g., the recent reviews[26,39] for more details about the progress on modelling gel-like colloidal particles.

In order to elucidate the properties of macroscopic systems such as nanogel stabilized emulsions, it is necessary to first understand how isolated soft particles behave at interfaces.[40] In this work, the correlation between the internal nanoparticle topology and its influence on

deformability, as well as solvent penetration at liquid-liquid interfaces is examined by means of MD simulations. For the first time this issue is addressed with excluded volume for all the interactions (liquid-liquid, monomer-monomer and cross-interactions) and the role of the network topology (disordered vs. regular) is investigated. Permeability is quantified by an unbiased analysis that counts the exact number of liquid particles inside the nanogel at every time. We find that such porous cavities do not exhibit nanoconfined homogeneous mixtures even for low interfacial strengths. Interestingly enough, the total liquid uptake and invasion (fraction of liquid within the nanogel at the other side of the interface) are optimized for a cross-linking degree that depends on the interfacial strength. Noticeably, the internal topology of the nanogel network (regular or disordered) does not seem to play a major role in the quality of the mixing, except for stiff interfaces where disordered networks show a higher efficiency.

The article is organized as follows. Section 2 describes the simulation details, while the main results and discussion are presented in sections 3 and 4. Finally in section 5 the conclusions and outlook are presented.

2 Computational Methodology

In this work, three different simulation stages have been considered, see Figure S1 in the supporting information (SI) for an overview of the whole workflow. First, the computational synthesis and equilibration of nanogels under implicit solvent conditions. Within such a stage, two families of homopolymeric nanogels were designed: one of them, generally employed in the literature, with a regular diamond-like network (from now on named ideal) and a second one with an irregular disordered network (from now on named realistic). In the latter case, nanogels were created with an in-house code following the methodology proposed in Refs.[34,41] In brief, the *in-silico* protocol resembles the design of nanogels, microgels[34] and globular single-chain nanoparticles,[41,42] as examples of soft polymeric objects. In order to

investigate the conformations and the effect of the internal network structure of the former particles on the mixing properties of immiscible liquids within nanocavities, we varied the fraction of internal crosslink densities, $f_{cl} = N_r/N_m$, with N_r and N_m the number of monovalent cross-linkable groups and the total number of monomers, respectively. This is indeed one of the crucial factors controlling nanogels behavior. This way, we tunned the elasticity of the nanogel to adapt itself at different interfacial strengths. In total, 4 types of nanogels were generated with f_{cl} = 3.9, 7.5, 14.0 and 19.9 %, respectively. Realistic nanogels were made of 2000 monomer units, and for the purpose of comparison, the ideal ones were as close as possible to the realistic ones; with 2000, 2002, 2021 and 2000 monomer units for each f_{cl} (more details on the ideal and realistic nanogels design can be found in Refs. 35 and 39 respectively). After the synthesis, such systems were equilibrated for 10^7 steps under Langevin dynamics.[43]

The second stage consisted of the generation and equilibration of nanogels at the interface between two inmiscible liquids with explicit fluid particles. For such, we placed the previous equilibrated nanogels at the center of the simulation box, and filled the box with two different liquids (A and B) of monoatomic molecules. Periodic boundary conditions were applied in all directions and the liquid/liquid interface was set in the $x - y$ plane and perpendicular to the z-direction. Nanogel's sizes were rationalized to have a good compromise between the large computational effort needed to include explicit solvent particles and the need of simulating large enough nanogels with a reasonable amount of solvent particles trapped in their interior. The PACKMOL package[44] was employed for generating the initial configuration of the system. Inside the cubic simulation box of sides $L = 100\sigma$, the two different fluid particles were packed with a particle number density $\rho^* \approx 0.952/\sigma^3$ (475000 particles for each liquid component + the nanogel). Finally, in order to provide reference conformations for comparisons at different environments (implicit solvent, as well as explicit solvent with monomer-solvent excluded volume interactions), at the third stage we make equal the cross-terms interactions between the liquids to simulate the case of a nanogel dis-

persed in an homogeneous mixture (single liquid). For the last two stages, systems were equilibrated for 10^9 steps. Through this paper, all simulations with explicit solvent were carried out with the GROMACS 4.6.5[45] package under Newtonian dynamics in the NVT ensemble. Lennard Jones reduced units are used, and all particle masses, energy and length scales are set as $m = \epsilon = \sigma = 1$. The reduced temperature and timescales, T^* an τ, are given by $T^* = \epsilon/k_B = 1$ (with k_B the Boltzmann constant) and $\tau = (m\sigma^2)^{1/2}$, respectively. The time step in all stages was $\delta t = 0.003\ \tau$, while the relaxation time for the Nosé-Hoover thermostat[46,47] was set to 0.5τ.

Concerning the interactions, these simulations employ the Kremer-Grest bead-spring model.[48] All non-bonded interactions between beads (nanogel's monomers and liquid particles) are given by the Weeks-Chandler-Anderson (WCA) potential[49] to account for excluded-volume interactions:

$$U^{WCA}(r) = 4\epsilon \left[\left(\frac{\sigma}{r}\right)^{-12} - \left(\frac{\sigma}{r}\right)^{-6} + \left(\frac{1}{4}\right) \right] \text{for} \quad r < 2^{1/6}\sigma \tag{1}$$

and zero for $r \geq 2^{1/6}\sigma$, while bonded nanogel's beads interact through the finite-extensible-non-linear spring (FENE) potential given by

$$U^{FENE}(r) = -\frac{1}{2} K_F R_0^2 \ln \left[1 - \left(\frac{r}{R_0}\right)^2 \right] \text{for} \quad r < R_0 \tag{2}$$

and ∞ for $r \geq R_0$, with $K_F = 15\sigma^{-2}$ and $R_0 = 1.5\sigma$. Thus, for dealing with a finite polymer network with m monomers, within a two-component mixture of explicit solvent molecules A and B, the interaction energy of the system is written as

$$U = \sum_{a,b,m=1}^{N_a,N_b,N_m} U^{WCA} + \sum_{bonds} U^{FENE} \tag{3}$$

where the purely repulsive nature of the WCA potential mimics good solvent conditions between the solvent and nanogel's monomers, while the combination of FENE and WCA

guarantees chain uncrossability by limiting the fluctuation of bonds in the nanogel. Additionally, we have considered the nanogel having the same affinity for both liquid components, $U^{WCA}(r_{ma}) = U^{WCA}(r_{mb}) = U^{WCA}(r_{mm})$. Such an assumption, very hard to implement in experiments, provides however a quasi-ideal scenario for investigating the effect of the network topology on the solvents' mixing inside the nanogel. Nonetheless, to account for the overall effect of interfacial fluctuations, 3 interaction strengths have been chosen for the liquid-liquid interactions ($\epsilon_{AB} = 3, 5$ and 15), while $\epsilon_{AB} = 1$ is considered the reference case for the homogeneous mixture (single liquid).

3 Results

3.1 Nanogel's deformability

In order to quantify the average nanogel's shape and size under different environments, the gyration tensor in the laboratory frame is employed and defined as

$$\mathrm{G}_{\mu\nu} = \frac{1}{2N_m^2} \sum_{i=1}^{N_m} \sum_{j=1}^{N_m} (r_\mu^{(i)} - r_\mu^{(j)})(r_\nu^{(i)} - r_\nu^{(j)}) \tag{4}$$

where the summation is performed over the N_m monomer beads in the nanogel, with $\mu, \nu \in \{x, y, z\}$ as the Cartesian coordinates of the i^{th}, j^{th} beads. Additionally, $\mathrm{G}_{\mu\nu}$ is also decomposed into perpendicular ($\mathrm{G}_\perp = \mathrm{G}_{zz}$) and parallel ($\mathrm{G}_\parallel = \mathrm{G}_{xx} + \mathrm{G}_{yy}$) components to obtain the size of the nanogels relative to their orientation at the interface. To describe the overall spatial distribution of monomers in the nanogels $\mathrm{G}_{\mu\nu}$ has to be diagonalized. After that, structural features are extracted by combining the corresponding eigenvalues ($\lambda_1 \geq \lambda_2 \geq \lambda_3$) into a group of shape parameters.[50,51] In this work, three of them are employed: The squared radius of gyration (${R_g}^2$),

$$\mathrm{Tr}\,\mathrm{G}_{\mu\nu} = \mathrm{G}_\perp + \mathrm{G}_\parallel = {R_g}^2 = \lambda_1 + \lambda_2 + \lambda_3 \tag{5}$$

as the sum of the principal moments. The asphericity (a)

$$a = \frac{(\lambda_2 - \lambda_1)^2 + (\lambda_3 - \lambda_1)^2 + (\lambda_3 - \lambda_2)^2}{2(\lambda_1 + \lambda_2 + \lambda_3)} \tag{6}$$

$0 \leq a \leq 1$, zero for symmetrical conformations (e.g. a sphere, a cube) and one meaning objects with cylindrical symmetry (e.g. a rod). The prolateness (p),

$$p = \frac{(3\lambda_1 - {R_g}^2)(3\lambda_2 - {R_g}^2)(3\lambda_3 - {R_g}^2)}{2(\lambda_1^2 + \lambda_2^2 + \lambda_3^2 - \lambda_1\lambda_2 - \lambda_1\lambda_3 - \lambda_2\lambda_3)^{3/2}} \tag{7}$$

$-1 \leq p \leq 1$, quantifies deviations between perfectly oblate ($p = -1$) and prolate ($p = 1$) objects.

In Figure 1 the main trends for the realistic and ideal nanogel are presented as a function of the degree of cross-linking and liquids compatibility, while Table S2 in the SI summarizes the average shape descriptors of nanogels under different environments. The radius of gyration has been decomposed into parallel and perpendicular components to quantify the nanogel's size (see top panels in Figure 1). The absence of explicit solvent leads to bigger nanogel's sizes (about 20%) than when it is embeded in the dense liquid, showing the relevance of excluded volume interactions even in the absence of the adsorbing interface. As the cross-link density increases, the nanogel's size decreases monotonically in the xy-plane and converges from above the $G_{\parallel}$ value of the homogeneous mixture case. No big differences are observed between the nanogels of both topologies and, except in the case $f_{cl} = 3.9$, the cross-linking degree has only a minor effect on the nanogel size when it is confined by the weakest interface ($\epsilon_{AB} = 03$) or solvated in the homogeneous mixture ($\epsilon_{AB} = 01$). Only for strong interfaces ($\epsilon_{AB} \geq 05$) the cross-linking degree plays a major role. In the z-direction, the nanogels show the opposite behavior and their size converges from below the $G_{\perp}$ of the homogeneous mixture case. For the weakest interface, the nanogel's perpendicular size remains almost constant while for $\epsilon_{AB} \geq 05$ it grows as the degree of cross-linking increases. Only when the degree of cross-linking is high the liquid compatibility has a minor effect on

$\dot{G}_{\perp}$ and $\dot{G}_{\parallel}$, otherwise nanogels deform according to how flexible their internal networks are.

The fact that nanogels can adapt their shapes to the confining environment is quantified by the asphericity and prolateness parameters. In particular, for the asphericity (see bottom-left panel in Figure 1), there is a clear trend toward spherical objects ($a \to 0$) as the degree of cross-linking grows. This indicates that nanogels are not able to deform anymore, no matter the strength of the interface. As the degree of cross-linking decreases and the interface becomes more rigid, nanogels lose the typical spherical shape found in the homogeneous mixture. The prolateness of such spheroidal objects (see bottom-right panel in Figure 1) describes how elongated (prolate) or flatened (oblate) the nanogels are when adsorbed at the interface or inmersed in the single liquid. For the latter, nanogels shows a prolateness close to zero as expected. Nevertheles, due to the inhomogeneous nature of realistic nanogel networks, they tend to have a more prolate character than their ideal counterparts. At the interface between two inmiscible liquids, nanogels gradually flaten as the strength of the interface increases and the degree of cross-linking decreases. For realistic nanogels, we again observe more elongated objects than for the regular networks as the number of cross-links and the interfacial strength increases. Due to the sensitivity of the prolateness, it seems that realistic nanogels are very different from their ideal counterparts, however if we plot the top and side view projections of the gyration tensor eigenvalues (see middle panels in Figure 1), such differences are less pronounced and now it is easier to appreciate the deformability of such soft objects. Overall, no significant differences are observed between realistic and ideal nanogels, except in the case of $f_{cl} = 3.9$ and ϵ_{AB} =15, which just indicates that the realistic nanogel is less deformable in the direction of the interfacial plane than its ideal counterpart. Figure S3 in the SI shows the parallel and perpendicular swelling curves, for the interfacial case against the nanogel dispersed in the homogeneous mixture. Clearly the most deformable nanogels (low f_{cl}) show the stronger dependence of their size on the interfacial strength.

More information on how the nanogels deform at the interface is gained by examining the average number density profiles $\rho(z)$ reported in Figure 2. In the case of the incompatible

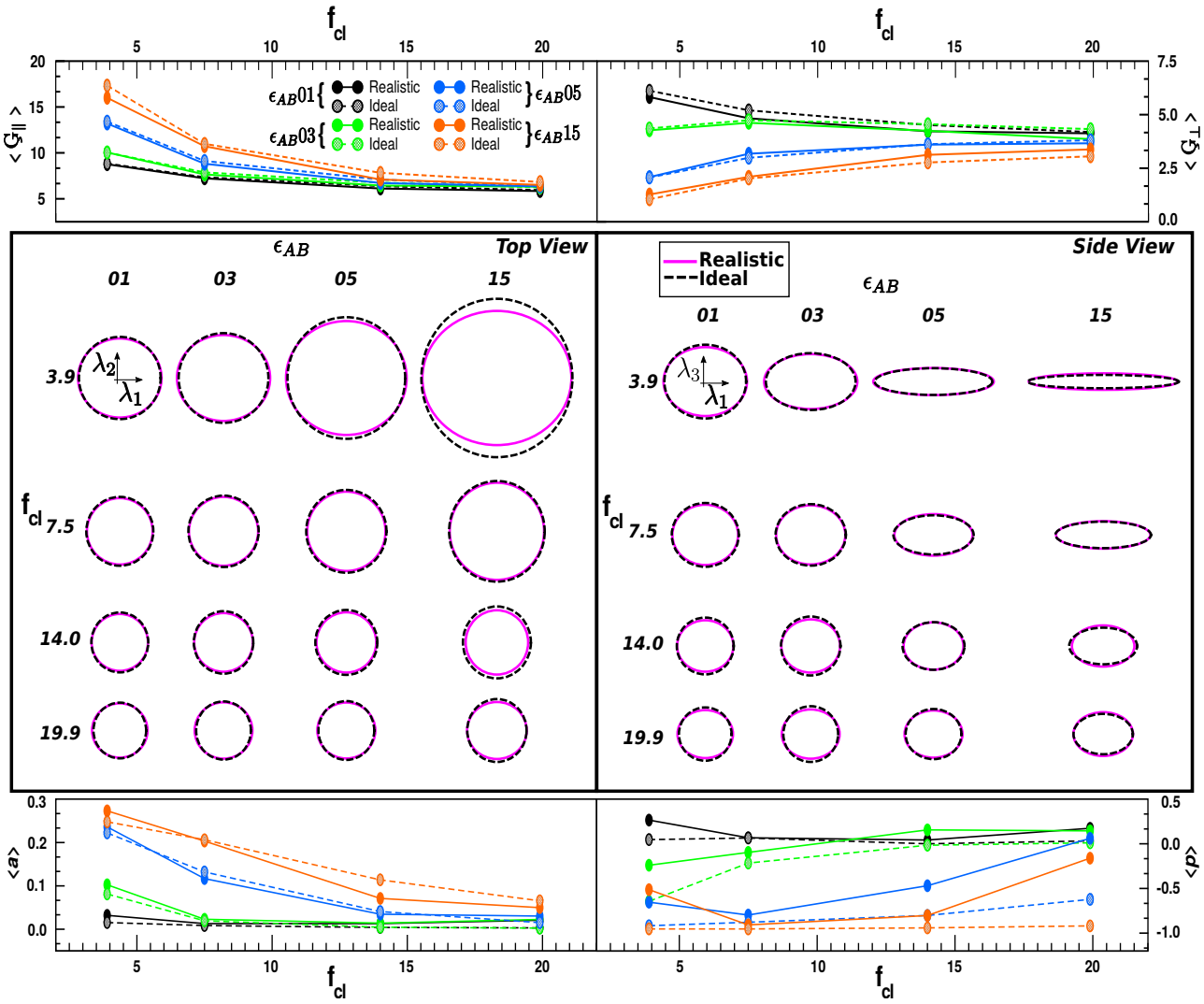

Figure 1: Shape parameters as a function of cross-link densities for different liquid compatibilities in realistic (continuous lines with solid circles) and ideal (dashed lines with textured circles) nanogels. Top panels represent the parallel (left) and perpendicular (right) decomposition of the radius of gyration. Middle panels correspond to the top (left) and side (right) view of the gyration ellipsoid (eigenvalues). Bottom panels correspond to the asphericity (left) and prolateness (right).

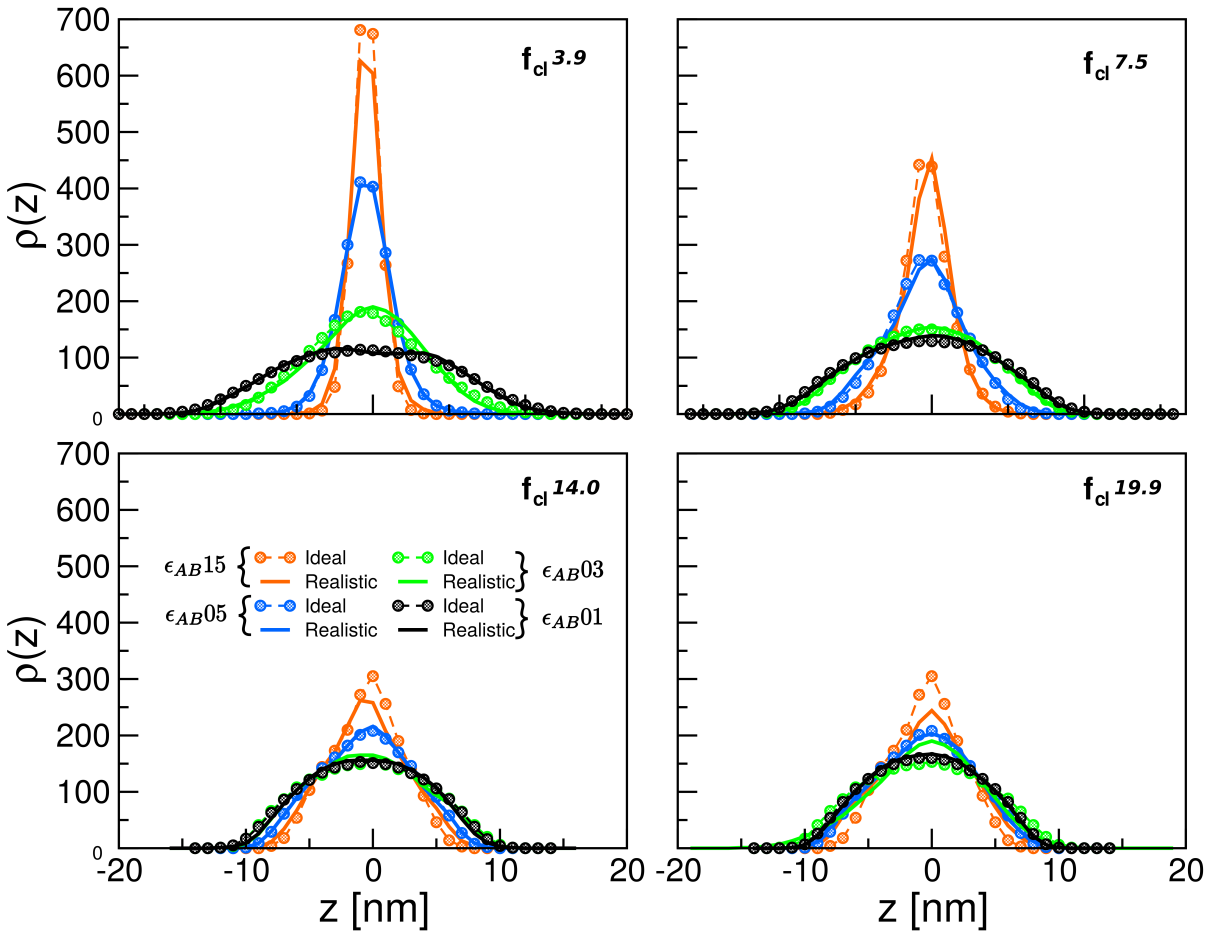

Figure 2: Density profiles of realistic (continuous lines) and ideal (dashed lines with textured circles) nanogels with f_{cl} = 3.9, 7.5, 14.0 and 19.9, taken orthogonally to the xy plane for different degrees of liquid's affinity: ϵ_{AB} = 01 corresponds to the single liquid, while ϵ_{AB} =03, 05 and 15 represent liquid mixtures with different degree of incompatibility. All data are normalized so that the area below the curve corresponds to the total number of particles in the nanogel.

liquids, such profiles measure the amount of nanogel monomers at a distance z from the interface, while for the case of nanogels immersed in the single liquid, such curves correspond to the number of nanogel monomers along the z coordinate in the simulation box. For the purpose of comparison, the homogeneous mixture will serve as a reference to highlight the differences between flattening or compression of nanogels when adsorbed at the interface.

For the nanogel dispersed in the single liquid, the distribution narrows as the degree of cross-linking increases. At the interface, nanogels' deformability comes from the interplay between the interfacial tension forces and the amount of structural nodes inside the nanogel. As expected, the maximum of $\rho(z)$ is found for $z = 0$ since nanogel monomers tend to reside at the interface in order to avoid direct contacts between the incompatible liquids. As aforementioned, the inhomogenous distribution of cross-links in realistic nanogels does not seem to significantly affect their overall shape when compared to their ideal counterparts. This also seems to be the case in terms of $\rho(z)$. However for very strong interfaces ($\epsilon_{AB} = 15$) the ideal nanogels generally accumulate more monomers in the interface ($z = 0$) than realistic ones. The shape of such profiles is strongly correlated with the side view projections presented in the middle-right panel of Figure 1. Further, there is a clear transition on how the nanogel monomers organize from the single liquid to the case of two inmiscible liquids. The central peaks decrease in intensity and broaden indicating that nanogels are less deformable and occupy more volume in the z-direction as the degree of cross-links increases. For very low degree of cross-linking the distributions narrow sharply as the interfacial strength increases, thus reaching a narrow peak that resembles a single layer of nanogel monomers.

3.2 Solvent penetration in deformable porous cavities

There are several ways to calculate how many solvent particles reside inside nanogels at each time frame. One might think that just using the components of the radius of gyration or the main ellipsoid axis to select the particles inside such boundaries would be sufficient. However such criteria might bias the interpretation for various reasons: (i) how one counts

the liquid particles will intrinsically depend on how one defines the enclosing surface that best describes the shape of the nanogel; (ii) even if in average the nanogel has an specific shape, it is important to pick up a geometric enclosing surface that also accounts for the instantaneous conformational fluctuations of the nanogel; (iii) and most importantly, the boundaries of such geometrical constructions correspond to an enclosing smooth surface and do not account for the nanogel protrusions of the outer layers. An alternative is to create a grid representation of the nanogel to count the number of solvent beads inside it. In particular, for each configuration we first construct an enclosing parallelogram surrounding the nanogel. The sides in all directions are selected so that the parallelogram encloses all the nanogel's monomers. Then we divide the parallelogram with a grid mesh size of $\Delta = \sigma$. For each column (x, y) in the grid we look for the highest and lowest nanogel's monomer in the $+z$ and $-z$ directions, respectively. During the panning, for each column (x, y) we count the cells with liquid beads (A or B) or nanogel monomers that are enclosed by the highest and lowest nanogel's monomers at that (x, y) (both monomers are also counted). In this way the counting considers the nanogel internal topology fluctuations, and does not count particles out of the nanogel's outer surface neither miss particles inside it —an artifact that emerges when a static smooth enclosing surface is used as, e.g., a sphere of radius $R_{\rm g} = \langle R_{\rm g}^2 \rangle^{1/2}$. Indeed our method, by construction, counts at every time the exact number of liquid particles that are inside the nanogel. In Figure S4, an instantaneous side view of the realistic nanogels is presented for the purpose of illustrating how the liquids reside inside the pores of such nanocavities. Additionally, two movies (S5 and S6 in the SI) show the side and top view projections of realistic and ideal nanogels with the solvent from bulk phases residing inside them.

Figure 3 shows the average relative amount of liquid particles A and B inside the nanogels, $\rho_a^{in(m)}$ and $\rho_b^{in(m)}$ respectively, in the perpendicular direction to the interface, while for the single liquid case profiles correspond to the z-axis of the simulation box. Two fractions of cross-links, 3.9 and 14.0 are presented here, while the remaining (f_{cl} =7.5 and f_{cl} =19.9) are

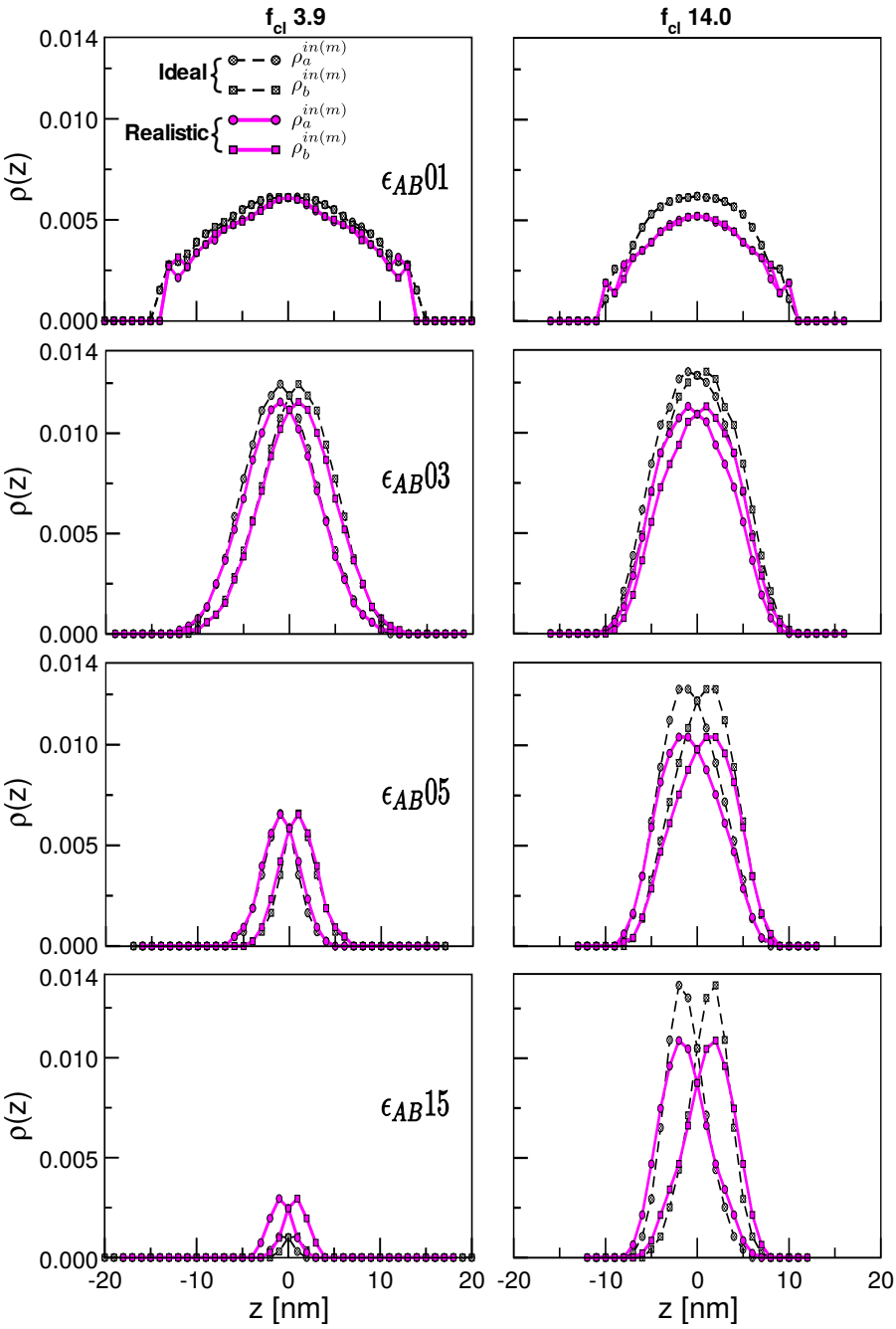

Figure 3: Density profile of solvent beads inside realistic and ideal nanogels. Liquids A and B correspond to $\rho_a^{in(m)} = \left\langle \frac{N_a^{in(m)}}{N_a^{in(m)}+N_b^{in(m)}+N_m} \right\rangle$ and $\rho_b^{in(m)} = \left\langle \frac{N_b^{in(m)}}{N_a^{in(m)}+N_b^{in(m)}+N_m} \right\rangle$ respectively. $N_{a,b}^{in(m)}$ and N_m denote the number of liquid (A or B) particles and nanogel monomers, respectively, inside the nanogel according to the grid representation. For each z-value all the counts of the different (x, y)-columns are summed, and averages are made over the different time frames. Curves are presented for the single liquid case as reference for comparison (upper panels), while the rest of the panels show the transition from the weakest to the strongest interfacial strength. The effects of the nanoparticle deformability are addressed from left to right, with f_{cl} =3.9 and f_{cl} =14.0 as examples of the lowest and intermediate cases of flexible nanocavities.

included in Figure S7 of the SI. To account for specific differences introduced by employing a homogenous or inhomogeneous distribution of nodes in the nanogel's internal network, curves have been normalized by the total sum of the nanogel's monomers and the liquids' particles inside such deformable objects. Their maxima do not lie at the center of the interface. Full overlap between $\rho_a^{in(m)}$ and $\rho_b^{in(m)}$ only occurs for the homogeneous mixture (upper panels). As the incompatibility between the liquids increases, the peak maxima separate from the interface and the liquids are also less miscible inside the nanogels. Additionally, the amount of liquids that the nanogel can retain for the case of highly incompatible liquids decreases considerably at low fractions of cross-links (f_{cl} =3.9), while for the rest of cross-linking degrees the curves reach a maximum of 0.014 for f_{cl} =7.5 (see Figure S7 of the SI) or remain almost constant as in the case of f_{cl} =14.0.

By comparing the differences between realistic and ideal nanogels, it is observed that a more homogeneous distribution of nodes in the internal structure leads immediately to an increase in nanogel's capacity (higher maxima). This is due to the fact that a regular node arrangement enhances the packing and distribute the liquids in a more efficient way. Such effects can be appreciated more clearly in Figure 4, where the uptake and invasive capacities of nanogels are represented, top and bottom panels respectively. The uptake is quantified by adding the areas below the curves in Figures 3 and S7. The invasive capacity is obtained by summing the areas below the $\rho_a^{in(m)}$ in the B-side ($\rho_a^{in(m_B)}$) and $\rho_b^{in(m)}$ in the A-side ($\rho_b^{in(m_A)}$), respectively, i.e., the liquid within the nanogel that is at the other side of the interface. For the single liquid case, the uptake capacity decreases in a monotonous way as the fraction of cross-links increases for both the realistic and ideal nanogels. This is an expected result as the nanogels become less deformable and therefore cannot swell to enclose more liquids inside them. For the immiscible liquids the trend shows a different behavior. For the weakest interface $\epsilon_{AB} = 03$ the uptake is weakly and non-monotonically dependent of the cross-linking degree, with a maximum at $f_{cl} \sim 5$. For higher interfacial strength, as the network becomes less deformable (higher f_{cl}) the uptake capacity increases

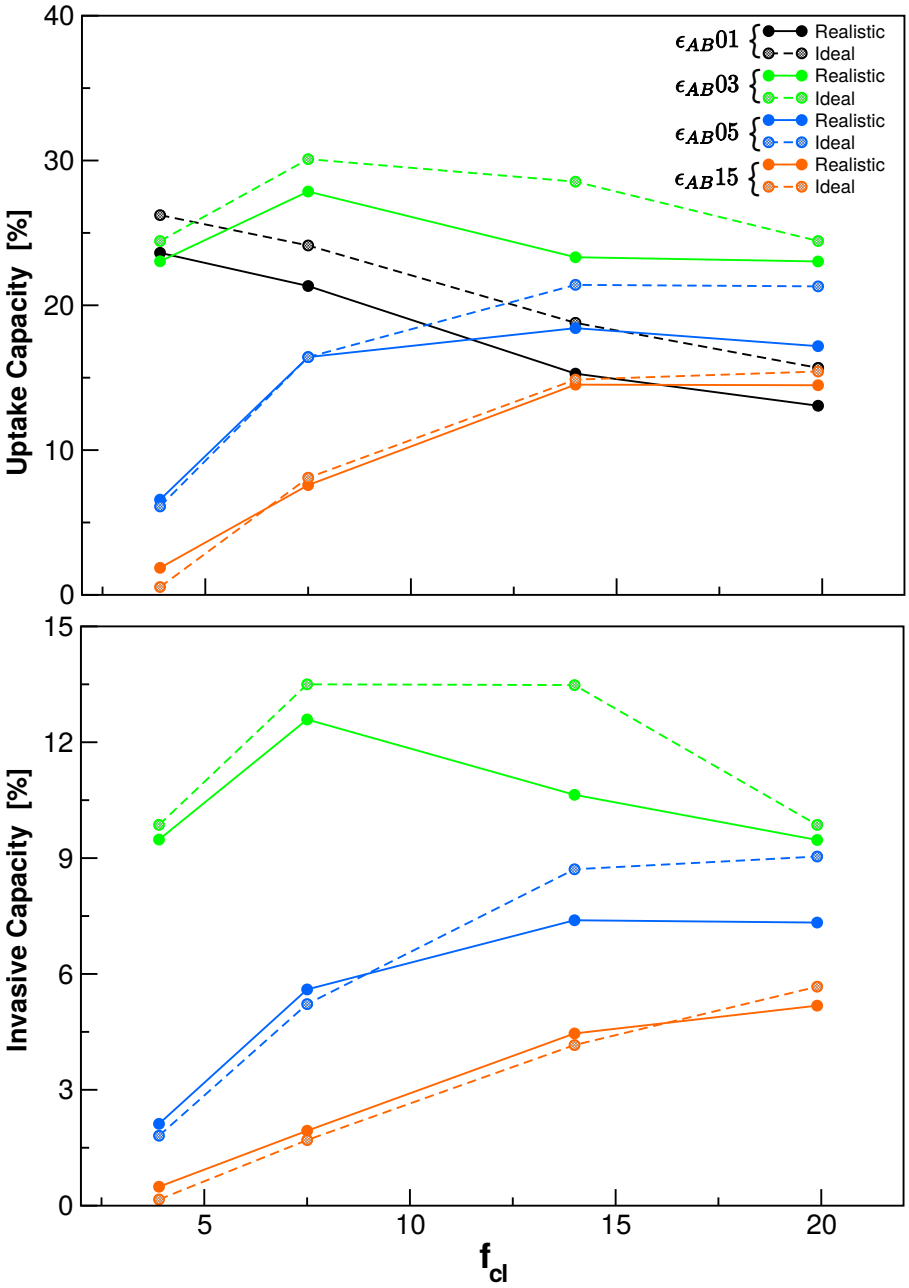

Figure 4: Solvent uptake $\left\langle \frac{N_a^{in(m)}+N_b^{in(m)}}{N_a^{in(m)}+N_b^{in(m)}+N_m} \right\rangle$ and invasive $\left\langle \frac{N_a^{in(B_m)}+N_b^{in(A_m)}}{N_a^{in(m)}+N_b^{in(m)}+N_m} \right\rangle$ capacities of liquids inside the realistic and ideal nanogels as a function of the particle deformability f_{cl} = 3.9, 7.5, 14.0 and 19.9, as well as the whole range of liquid compatibilities employed in this study. $N_\alpha^{in(\beta_m)}$ denotes the 'invasive' α-liquid particles, i.e., those inside the nanogel that are at the β-side of the interface.

until reaching a plateau where nanogels cannot accommodate more liquids, no matter the degree of cross-linking. It is obviously expected that if the number of nodes in the network further increases, the capacity to capture solvent inside their cavities will drop at some point, until reaching the limit case of a rigid nanoparticle (no uptake). In terms of the total mass (nanogel monomers and the liquids inside them), we observe that the invasive capacity (A-liquid in the B-side and *viceversa*) follows a trend that is very similar to the uptake capacity. Indeed it appears that for the weakest interface almost half of the solvent particles inside the nanogel are residing on the other side of the interface.

Given such a strong correlation, in Figure 5 we present the ratio between the invasive and uptake capacity to quantify the quality of mixing (i.e., which fraction of the total liquid captured by the nanogel is at the other side of the interface). Moreover, we also include the mixing capacity outside the nanogel, i.e., the fraction of interfacial liquid at the other side of the bare interface. This was done to verify if miscibility is really enhanced inside the cavities of such deformable particles. A simulation at the same number density but with no nanogel was carried out for calculating the mixing capacity in the bare interface. For the sake of a fair comparison, the integration limits in the bare interface were taken as those of the average nanogel size in the $\pm z$ directions. For all the interfacial strengths we observe a clear enhancement of the miscibility of solvent particles inside the nanogel with respect to that in the bare interface (see Figure 6). For the weakest interface, such enhancement ($\approx$ 2.5 factor) is almost independent on the degree of cross-linking, while for the other interfaces the miscibility inside the nanogel increases considerably from a factor of 2-2.5 for both the intermediate and rigid interfaces at low f_{cl} =3.9, to almost a factor of 3.5-5 at high degree of cross-linking f_{cl} =19.9. By comparing the mixing capacity between realistic and ideal nanogels, we observe that for the weakest interface there is no significant differences between them, while for the rigid interface the realistic nanogel shows a considerably better capacity of mixing.

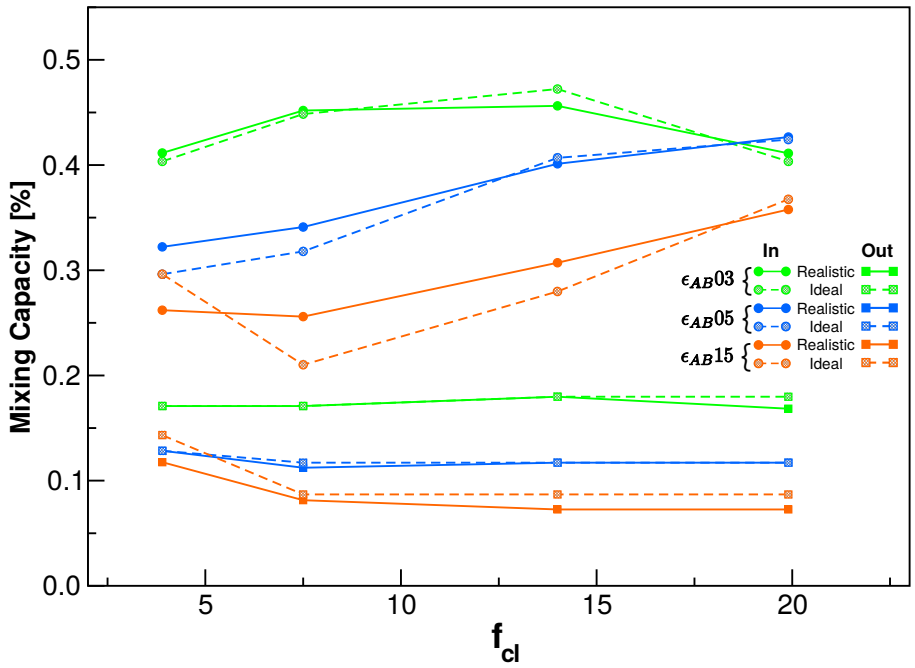

Figure 5: Quality of mixing $\left\langle \frac{N_a^{in(m_B)}+N_b^{in(m_A)}}{N_a^{in(m)}+N_b^{in(m)}} \right\rangle$ inside and outside of realistic and ideal nanogels as a function of particle deformability f_{cl} = 3.9, 7.5, 14.0 and 19.9, and for the whole range of interfacial strengths.

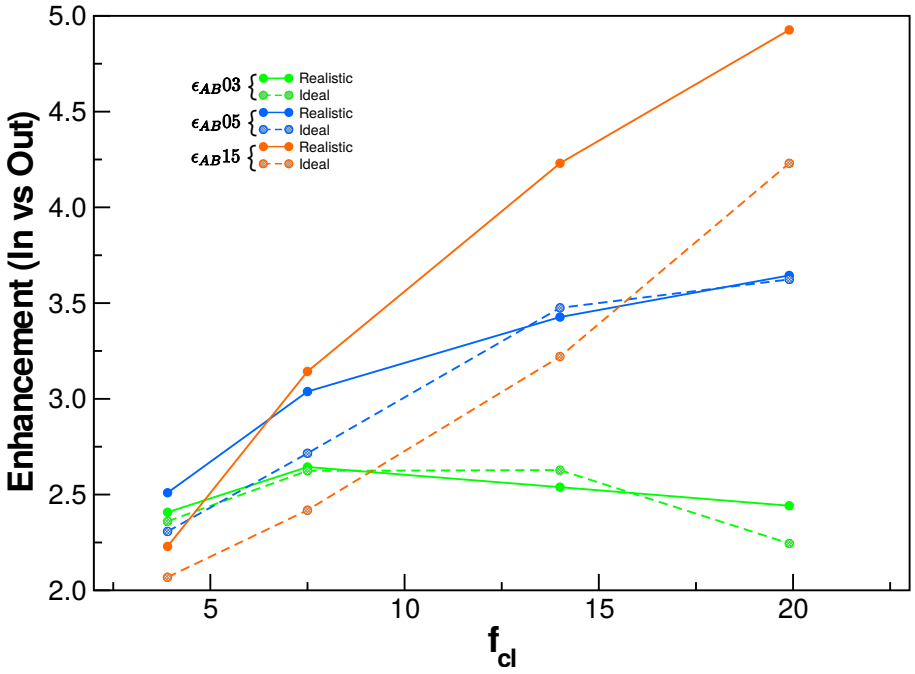

Figure 6: Miscibility enhancement for realistic and ideal nanogels as a function of the density of cross-links. Such curves correspond to the ratios between the quality of mixing inside and outside the nanogels, and they are represented for the whole range of interfacial strengths

4 Discussion

Before continuing let us recall that up to date the focus of simulations and experiments has been oriented towards explaining structural properties of microgels in suspensions or at interfaces. Only a few recent works have addressed the question of the liquids' miscibility inside the microgel.[30–33] The influence of the network topology in features such as softness, particle permeability and their correlation is discussed here for large-scale simulations with explicit solvent molecules and excluded volume interactions. Previous experimental studies[11,52–54] show that the resistance or fragility of emulsions generated with analogous particles in the micro scale depends on many factors such as: (i) the cross-link density, (ii) the size, (iii) the arrangement and packaging, as well as (iv) the processing or emulsification pathway. All of them from one way or another apparently modulate deformability, which is the key factor that differentiates soft from hard particles. Nevertheless, the impact on interfacial properties is not clear yet as there are some discrepancies concerning if deformability really facilitates adsorption and consequently enhance emulsion stability.[11,14,55] Ref.[52] has reported that if the size of microgels is increased for a fixed cross-link density, this immediately leads to a decrease in surface coverage, in turn deteriorating emulsion stability. Under the former assumption, small microgels or nanogels could offer additional advantages such as a better bridging inhibition, films that withstand mechanical stress and ultimately more handleable emulsions.

In this work, deformability was accessed by changing the density of cross-links. It has been demonstrated that it is the governing parameter in emulsions stabilized with small microgels.[52] Their morphology can also be manipulated through different interfacial strengths. For instance, highly deformed particles were found in our simulations for nanogels adsorbed at very rigid interfaces. Such conformations are analogous to those observed in emulsions under high shear rates.[56] Despite that our nanogels have the same affinity for both liquids, we still observe their characteristic broadening at the interface as the degree of cross-links increases. Indeed, our polymer density profiles correlate very well with the results reported

for microgels with fried-egg-like shapes.[28,29,52,57] Even though these simulations correspond to nanogels that are far from the overlap concentration, such deformable objects are intrinsically permeable. This implies that droplet adhesion can be facilitated or inhibited by tunning the invasive capacity of such particles. As we saw in the previous section, the invasive capacity is reduced for highly deformable nanogels. In this context, nanogels have an additional advantage with respect to their counterparts in the microscale as their invasive capacity will depend on the object size and shape —the extent of invasion is limited to distances much smaller than typical microgel sizes, except close to the limit of miscibility. For the case of densely packed nanogels, we expect that this quantity will have few variations and it might help to explain why single nanogel monolayers are more adhesive than emulsion droplets made with thicker barriers.[53]

Regarding solvent penetrability, particularly in the context of mixing, Potenkim *et al.*[30,31,33] showed that liquid miscibility is higher within ideal microgels than in the bulk, and that liquids inside them can be in a partial or fully mixed state. The results presented in this study go in the same direction, however there are noticeable differences between the liquid density profiles presented in this work, and those reported by Refs.[30,31,33] In particular, no homogeneous mixing is observed inside the nanogels for the whole range of cross-links and interfacial strengths employed in this study (in contrast to the flat profiles observed in such references for low or moderate interfacial strength). This indicates, first, that smooth geometrical enclosing volumes[30,31,33] are not the best choice to discriminate solvent particles inside porous nanocavities, since they do not capture the fluctuations of the microgel's surface and easily count for liquid particles that are close but out of the microgel. The grid representation approach presented in this work offers a suitable and unbiased choice to select solvent particles inside soft nanoparticles with strong deformability. How the solvent particles are modeled is another source of discrepancies. In fact, the introduction of explicit solvent particles with excluded volume interactions immediately rules out the possibility of liquid overlapping in the simulation cell and, more importantly, inside the nanogel's cavities.

Modelling the solvent with a dissipative particle potential facilitates analogies with Flory-Huggins lattice models.[31] However care must be taken as the ultrasoft and bound character of such a potential, and the high density of DPD particles inherent to the method, allow for liquid particle overlapping. This is especially critical inside the polymeric nanoparticles, where bulk solvent can permeate more easily due to screening of non-favorable contacts via the polymer monomers. DPD interactions have aso been used for the monomer-monomer interactions in the diamond networks of Refs.[30,31,33] However, the use of excluded volume for the monomer-monomer interactions is essential to investigate the nanogels, at least for disordered networks, since in these systems bounded DPD interactions will easily lead to violation of topological constraints (entanglements) through chain crossing, especially when the nanogel flatens at the interface. Finally, if we think about the specific role of network topology (ideal vs realistic nanogels), caution is advised particularly from the experimental point of view as the community is rapidly transitioning from simple, approximately homogeneous gel particles towards more sophisticated realizations, e.g. in terms of chemistry, architecture and softness.[21,33] As our results indicate, network topology does not seem to critically influence the quality of mixing. Our simulations show that realistic disordered nanogels even have, for intermediate and very rigid interfaces, slightly better mixing capacities than ideal regular networks. Therefore rushing to enhance their efficiency by tunning the network topology should be seen with some skepticism. From another perspective, even if the internal nanogel topology does not critically influence mixing (realistic vs ideal), we believe that this will be an important factor in emulsion stability. For instance, it would be interesting to push forward more complex nanoparticle architectures to examine if enhanced mechanical properties are observed in the densely packed responsive monolayers of nanogel or microgel stabilized emulsions.[8,21,58]

5 Conclusions

We have presented a systematic and intensive computational study to understand the conformational properties of a soft colloidal particle (nanogel) adsorbed at the interface between two inmiscible liquids. We have synthetized realistic and ideal nanogels *in-silico* with different degrees of cross-linking. To investigate how a regular and a disordered distribution of the network's nodes influences the internal resistance to deformation, molecular dynamics simulations have been performed with explicit solvent molecules and with excluded volume for all the interactions. At the interface between two inmiscible liquids, nanogels adopt a shape that depends on the amount of nodes in their network and the interfacial tension of the confining medium.

The nanogel permeability was analyzed by making use of a grid representation that picks the exact number of solvent particles inside deformable objects. With such an unbiased approach, it has been possible to obtain reliable density profiles for liquids inside such porous nanocavities. Comparisons were provided with respect to the case of a particle immersed in a single liquid. Nanogel's permeability is intrinsically related to the particle deformability. For a specific fraction of cross-links, the uptake of solvent particles in ideal nanogels is significantly bigger than their realistic counterpart due to its better packing efficiency. As the nanogels become less deformable, their uptake capacity reaches a plateau that depends on the interfacial forces between both liquids. Overall, the solvent uptake is optimized for cross-linking density $\sim 5\%$ at soft interfaces and for $\sim 15 - 20\%$ at moderate and stiff interfaces.

We did not observe a fully mixed state for any of the interfacial strengths and degrees of cross-linking investigated, not even at soft interfaces. This is contrary to what is reported via mean field approximations,[30] or even with mesoscopic DPD simulations.[31,33] Therefore our results suggest the need of incorporating the excluded volume for all the interactions (liquid-liquid, monomer-monomer and cross-interactions) to investigate liquid miscibility within soft nanoparticles. The results reported in this study indicate that miscibility is

largely enhanced inside the nanocavities with respect to the bulk. In particular, we find that the mixing quality is enhanced by a factor between 2 and 5, depending on the degree of cross-linking and the interfacial strength. Most importantly, the specific network topology only influences significantly the mixing quality for rigid interfaces, the disordered network providing a better mixing.

The emerging scenario proposes general guidelines, not only for setting the shape, uptake and mixing capacity of nanogels adsorbed at liquid-liquid interfaces, but also for tuning the invasive capacity, which is an essential element to control the catalysis rates in interfacial soft nanoreactors. Furthermore, the results reported here should motivate future studies to unravel the specific role of the nanogel's instrinsic permeability within armored and bridging droplets. Work in this direction in progress.

Acknowledgement

DJAA acknowledges the career funding support from the DIPC foundation. This work has been supported by the projects PGC2018-094548-B-I00 (MCIU/AEI/FEDER, UE) and IT-1175-19 (Basque Government, Spain).

Supporting Information Available

The following files are available free of charge. The following files are included to support the findings of this study

- S1 (Figure): Overview of the computational workflow
- S2 (Tables): Average shape parameters of nanogels under different environments.
- S3 (Figure): Swelling curves of nanogels in the perpendicular and parallel direction to the interface.

- S4 (Figure): Snapshot of solvent particles residing inside nanogels.
- S5-S6 (Videos): Side and top view videos for liquids inside nanogels.
- S7 (Figure): Density profiles of liquids inside nanogels with 7.5 and 19.9 cross-links fractions.

References

(1) Karg, M.; Pich, A.; Hellweg, T.; Hoare, T.; Lyon, L. A.; Crassous, J. J.; Suzuki, D.; Gumerov, R. A.; Schneider, S.; Potemkin, I. I.; Richtering, W. Nanogels and Microgels: From Model Colloids to Applications, Recent Developments, and Future Trends. *Langmuir* **2019**, *35*, 6231–6255.

(2) Gupta, S.; Camargo, M.; Stellbrink, J.; Allgaier, J.; Radulescu, A.; Lindner, P.; Zaccarelli, E.; Likos, C. N.; Richter, D. Dynamic phase diagram of soft nanocolloids. *Nanoscale* **2015**, *7*, 13924–13934.

(3) Stuart, M. A. C.; Huck, W. T.; Genzer, J.; Müller, M.; Ober, C.; Stamm, M.; Sukhorukov, G. B.; Szleifer, I.; Tsukruk, V. V.; Urban, M.; Winnik, F.; Zauscher, S.; Luzinov, I.; Minko, S. Emerging applications of stimuli-responsive polymer materials. *Nature Materials* **2010**, *9*, 101–113.

(4) Plamper, F. A.; Richtering, W. Functional microgels and microgel systems. *Accounts of Chemical Research* **2017**, *50*, 131–140.

(5) Agrawal, G.; Agrawal, R. Stimuli-responsive microgels and microgel-based systems: Advances in the exploitation of microgel colloidal properties and their interfacial activity. *Polymers* **2018**, *10*, 418.

(6) Echeverria, C.; Fernandes, S. N.; Godinho, M. H.; Borges, J. P.; Soares, P. I. Functional stimuli-responsive gels: Hydrogels and microgels. *Gels* **2018**, *4*, 54.

(7) Thorne, J. B.; Vine, G. J.; Snowden, M. J. Microgel applications and commercial considerations. *Colloid and Polymer Science* **2011**, *289*, 625.

(8) Deshmukh, O. S.; van den Ende, D.; Stuart, M. C.; Mugele, F.; Duits, M. H. Hard and soft colloids at fluid interfaces: Adsorption, interactions, assembly & rheology. *Advances in Colloid and Interface Science* **2015**, *222*, 215–227.

(9) Serpe, M. J. Fine-tuned gel particles enable smart windows for energy efficiency. 2019.

(10) Torres, O.; Andablo-Reyes, E.; Murray, B. S.; Sarkar, A. Emulsion microgel particles as high-performance bio-lubricants. *ACS Applied Materials & Interfaces* **2018**, *10*, 26893–26905.

(11) Schmitt, V.; Ravaine, V. Surface compaction versus stretching in Pickering emulsions stabilised by microgels. *Current Opinion in Colloid & Interface Science* **2013**, *18*, 532–541.

(12) Yunker, P. J.; Chen, K.; Gratale, M. D.; Lohr, M. A.; Still, T.; Yodh, A. Physics in ordered and disordered colloidal matter composed of poly (N-isopropylacrylamide) microgel particles. *Reports on Progress in Physics* **2014**, *77*, 056601.

(13) Kwok, M.-h.; Sun, G.; Ngai, T. Microgel Particles at Interfaces: Phenomena, Principles, and Opportunities in Food Sciences. *Langmuir* **2019**, *35*, 4205–4217.

(14) Murray, B. S. Microgels at fluid-fluid interfaces for food and drinks. *Advances in Colloid and Interface Science* **2019**, 101990.

(15) Ngai, T.; Bon, S. A. *Particle-stabilized emulsions and colloids: formation and applications*; Royal Society of Chemistry, 2014.

(16) Gupta, A.; Eral, H. B.; Hatton, T. A.; Doyle, P. S. Nanoemulsions: formation, properties and applications. *Soft Matter* **2016**, *12*, 2826–2841.

(17) Wu, N.; Lee, D.; Striolo, A. *Anisotropic Particle Assemblies: Synthesis, Assembly, Modeling, and Applications*; Elsevier, 2018.

(18) Sicard, F.; Toro-Mendoza, J.; Striolo, A. Nanoparticles Actively Fragment Armored Droplets. *ACS Nano* **2019**, *13*, 9498–9503.

(19) Ngai, T.; Behrens, S. H.; Auweter, H. Novel emulsions stabilized by pH and temperature sensitive microgels. *Chemical Communications* **2005**, 331–333.

(20) Wiese, S.; Tsvetkova, Y.; Daleiden, N. J.; Spieß, A. C.; Richtering, W. Microgel stabilized emulsions: Breaking on demand. *Colloids and Surfaces A: Physicochemical and Engineering Aspects* **2016**, *495*, 193–199.

(21) Richtering, W.; Saunders, B. R. Gel architectures and their complexity. *Soft Matter* **2014**, *10*, 3695–3702.

(22) Siemes, E.; Nevskyi, O.; Sysoiev, D.; Turnhoff, S. K.; Oppermann, A.; Huhn, T.; Richtering, W.; Wöll, D. Nanoscopic visualization of cross-linking density in polymer networks with diarylethene photoswitches. *Angewandte Chemie International Edition* **2018**, *57*, 12280–12284.

(23) Karanastasis, A. A.; Zhang, Y.; Kenath, G. S.; Lessard, M. D.; Bewersdorf, J.; Ullal, C. K. 3D mapping of nanoscale crosslink heterogeneities in microgels. *Materials Horizons* **2018**, *5*, 1130–1136.

(24) Geisel, K.; Isa, L.; Richtering, W. Unraveling the 3D localization and deformation of responsive microgels at oil/water interfaces: a step forward in understanding soft emulsion stabilizers. *Langmuir* **2012**, *28*, 15770–15776.

(25) Cristofolini, L.; Orsi, D.; Isa, L. Characterization of the dynamics of interfaces and of interface-dominated systems via spectroscopy and microscopy techniques. *Current Opinion in Colloid & Interface Science* **2018**, *37*, 13–32.

(26) Martín-Molina, A.; Quesada-Pérez, M. A review of coarse-grained simulations of nanogel and microgel particles. *Journal of Molecular Liquids* **2019**, *280*, 374–381.

(27) Krüger, T.; Frijters, S.; Günther, F.; Kaoui, B.; Harting, J. Numerical simulations of complex fluid-fluid interface dynamics. *The European Physical Journal Special Topics* **2013**, *222*, 177–198.

(28) Camerin, F.; Gnan, N.; Rovigatti, L.; Zaccarelli, E. Modelling realistic microgels in an explicit solvent. *Scientific Reports* **2018**, *8*, 14426.

(29) Camerin, F.; Fernández-Rodríguez, M. Á.; Rovigatti, L.; Antonopoulou, M.-N.; Gnan, N.; Ninarello, A.; Isa, L.; Zaccarelli, E. Microgels Adsorbed at Liquid–Liquid Interfaces: A Joint Numerical and Experimental Study. *ACS nano* **2019**, *13*, 4548–4559.

(30) Rumyantsev, A. M.; Gumerov, R. A.; Potemkin, I. I. A polymer microgel at a liquid–liquid interface: theory vs. computer simulations. *Soft Matter* **2016**, *12*, 6799–6811.

(31) Gumerov, R. A.; Rumyantsev, A. M.; Rudov, A. A.; Pich, A.; Richtering, W.; Moller, M.; Potemkin, I. I. Mixing of two immiscible liquids within the polymer microgel adsorbed at their interface. *ACS Macro Letters* **2016**, *5*, 612–616.

(32) Gumerov, R. A.; Rudov, A. A.; Richtering, W.; Moller, M.; Potemkin, I. I. Amphiphilic arborescent copolymers and microgels: from unimolecular micelles in a selective solvent to the stable monolayers of variable density and nanostructure at a liquid Interface. *ACS applied materials & interfaces* **2017**, *9*, 31302–31316.

(33) Gumerov, R. A.; Filippov, S. A.; Richtering, W.; Pich, A.; Potemkin, I. I. Amphiphilic microgels adsorbed at oil–water interfaces as mixers of two immiscible liquids. *Soft matter* **2019**, *15*, 3978–3986.

(34) Moreno, A. J.; Lo Verso, F. Computational investigation of microgels: synthesis and effect of the microstructure on the deswelling behavior. *Soft Matter* **2018**, *14*, 7083–7096.

(35) Gnan, N.; Rovigatti, L.; Bergman, M.; Zaccarelli, E. In silico synthesis of microgel particles. *Macromolecules* **2017**, *50*, 8777–8786.

(36) Minina, E. S.; Sánchez, P. A.; Likos, C. N.; Kantorovich, S. S. Studying synthesis confinement effects on the internal structure of nanogels in computer simulations. *Journal of Molecular Liquids* **2019**, *289*, 111066.

(37) Ninarello, A.; Crassous, J. J.; Paloli, D.; Camerin, F.; Gnan, N.; Rovigatti, L.; Schurtenberger, P.; Zaccarelli, E. Modeling Microgels with a Controlled Structure across the Volume Phase Transition. *Macromolecules* **2019**, *52*, 7584–7592.

(38) Rudyak, V. Y.; Kozhunova, E. Y.; Chertovich, A. V. Towards the realistic computer model of precipitation polymerization microgels. *Scientific Reports* **2019**, *9*, 13052.

(39) Rovigatti, L.; Gnan, N.; Tavagnacco, L.; Moreno, A. J.; Zaccarelli, E. Numerical modelling of non-ionic microgels: an overview. *Soft matter* **2019**, *15*, 1108–1119.

(40) Ballard, N.; Law, A. D.; Bon, S. A. Colloidal particles at fluid interfaces: behaviour of isolated particles. *Soft matter* **2019**, *15*, 1186–1199.

(41) Lo Verso, F.; Pomposo, J.; Colmenero, J.; Moreno, A. Simulation guided design of globular single-chain nanoparticles by tuning the solvent quality. *Soft Matter* **2015**, *11*, 1369–1375.

(42) Pomposo, J. *Single-Chain Polymer Nanoparticles: Synthesis, Characterization, Simulations, and Applications*; Wiley, 2017.

(43) Allen, M. P.; Tildesley, D. J. *Computer simulation of liquids*; Oxford University Press, 2017.

(44) Martinez, L.; Andrade, R.; Birgin, E. G.; Martinez, J. M. PACKMOL: A package for building initial configurations for molecular dynamics simulations. *Journal of Computational Chemistry* **2009**, *30*, 2157–2164.

(45) Abraham, M. J.; Murtola, T.; Schulz, R.; Pall, S.; Smith, J. C.; Hess, B.; Lindahl, E. GROMACS: High performance molecular simulations through multi-level parallelism from laptops to supercomputers. *SoftwareX* **2015**, *1–2*, 19–25.

(46) Shuichi, N. A molecular dynamics method for simulations in the canonical ensemble. *Molecular Physics* **1984**, *52*, 255–268.

(47) Hoover, W. G. Canonical dynamics: Equilibrium phase-space distributions. *Phys. Rev. A* **1985**, *31*, 1695–1697.

(48) Kremer, K.; Grest, G. S. Dynamics of entangled linear polymer melts: A molecular-dynamics simulation. *J. Chem. Phys.* **1990**, *92*, 5057–5086.

(49) Weeks, J. D.; Chandler, D.; Andersen, H. C. Role of Repulsive Forces in Determining the Equilibrium Structure of Simple Liquids. *The Journal of Chemical Physics* **1971**, *54*, 5237–5247.

(50) Rawdon, E. J.; Kern, J. C.; Piatek, M.; Plunkett, P.; Stasiak, A.; Millett, K. C. Effect of knotting on the shape of polymers. *Macromolecules* **2008**, *41*, 8281–8287.

(51) Rudnick, J.; Gaspari, G. The shapes of random walks. *Science* **1987**, *237*, 384–389.

(52) Destribats, M.; Eyharts, M.; Lapeyre, V.; Sellier, E.; Varga, I.; Ravaine, V.; Schmitt, V. Impact of pNIPAM microgel size on its ability to stabilize Pickering emulsions. *Langmuir* **2014**, *30*, 1768–1777.

(53) Keal, L.; Lapeyre, V.; Ravaine, V.; Schmitt, V.; Monteux, C. Drainage dynamics of thin liquid foam films containing soft PNiPAM microgels: influence of the cross-linking density and concentration. *Soft Matter* **2017**, *13*, 170–180.

(54) Tatry, M. C.; Laurichesse, E.; Perro, A.; Ravaine, V.; Schmitt, V. Kinetics of spontaneous microgels adsorption and stabilization of emulsions produced using microfluidics. *Journal of colloid and interface science* **2019**, *548*, 1–11.

(55) Destribats, M.; Lapeyre, V.; Wolfs, M.; Sellier, E.; Leal-Calderon, F.; Ravaine, V.; Schmitt, V. Soft microgels as Pickering emulsion stabilisers: role of particle deformability. *Soft Matter* **2011**, *7*, 7689–7698.

(56) Destribats, M.; Wolfs, M.; Pinaud, F.; Lapeyre, V.; Sellier, E.; Schmitt, V.; Ravaine, V. Pickering emulsions stabilized by soft microgels: influence of the emulsification process on particle interfacial organization and emulsion properties. *Langmuir* **2013**, *29*, 12367–12374.

(57) Harrer, J.; Rey, M.; Ciarella, S.; Lowen, H.; Janssen, L. M.; Vogel, N. Stimuli-responsive behavior of PNiPAm microgels under interfacial confinement. *Langmuir* **2019**, *35*, 10512–10521.

(58) Maestro, A. Tailoring the interfacial assembly of colloidal particles by engineering the mechanical properties of the interface. *Current opinion in colloid & interface science* **2019**, *39*, 232–250.